Segmentation of Soft Tissues in Medical Images

Term Paper
Submitted to School of Computing
for Ph.D. Qualifying Examination

by

Ding Feng (H040297J)

under guidance of

Dr. Leow Wee Kheng (Associate Professor)

School of Computing
National University of Singapore

April 2005

Abstract

Medical image segmentation, as an application of image segmentation, is to extract some anatomial structures from various medical image modalities. Some major medical image modalities include CT (Computed Tomography), MRI (Magnetic Resonance Imaging) and PET (Positron Emission Tomography). In this paper, we classify the existing medical image segmentation techniques into several categories and give a thorough review of the related literatures. Their pros and cons are analyzed. Some possible research topics are dicussed. Some preliminary work is also presented and the experimental results are discussed.

Acknowledgement

I want to thank my supervisor, A/Professor Leow Wee Kheng, who gave me invaluable advice for writing this term paper.

I also thank Ruixuan Wang, Piyush Kanti Bhunre Dennis Lim Shere, Ying Chen, Xiaoping Miao and Sheng Zhang for their precious comments and suggestions.

List of Figures

List of Tables

Contents

Chapter 1

Introduction

1.1 Motivation

Medical Imaging technologies, such as CT, MRI and PET, have been widely applied to various medical procedures. Compared to traditional medical diagnosis, they provide non-invasive yet powerful means to investigate the internal structures and activities of human bodies. With the help of such technologies, doctors can obtain multi-dimensional information such as 2-D slices, 3-D volumetric images and videos of regions of interest (ROI), which facilitates the performance of both qualitative and quantitative analysis. This analysis provides invaluable information for diagnosis as well as surgical planning, thus may relieve the pains for the patients to some extent. Some sample cross-sectional abdominal CT images are shown in Figure 1.2 and 1.4.

Medical image segmentation is usually the first step of most analysis procedures mentioned above. It is also a crucial step that determines the final result of the entire application, since the rest of the analysis fully relies on the data from this step. For example, to build a 3-D volumetric model from a series of medical images, segmentation in 2-D images should be as accurate as possible; otherwise, the volume of the reconstructed model will be wrong, and visualization of this model will be meaningless. Subsequent medical processing and analysis steps may include quantification, registration, visualization and computer aided diagnosis. Regions of interest may include brain, bone structures, vessels, soft tissues, etc.

Medical image segmentation can be used in various applications. For example, in the application of cardiac diagnosis, given the segmentation of cardiac tissues in consecutive slices, 3-D volumetric models of the heart and blood vessels can be reconstructed. By modeling the blood flow inside, doctors can pinpoint the heart problem and assess the risk quantitatively. 3-D visualization of heart can further aid doctors to make assessment.

1.1.1 Objective

The problem of image segmentation can be formulated as follows. Given image $I = \{p_i\}$, a complete segmentation problem is to determine connected subset R_i ($R_i \subset I$), such that

$$\bigcup_i R_i = I, \quad R_i \cap R_j = \emptyset \quad (i \neq j). \tag{1.1.1}$$

Segmentation is based on homogeneity of the image characteristics such as intensitiy, color, texture, or the combination of all these information.

For medical image segmentation, the second condition mentioned above is not necessarily met. For instance, in X-ray images, body structures are sometimes overlapped. Figure 1.1 shows such an X-ray image that the contours of some hand bones are overlapped.

This is not the case for other medical image modalities such as CT images, which will be focused on in this paper. Hereafter, we will discuss the medical image segmentation problem in the context of CT images.

Broadly speaking, medical image segmentation has two sorts of objectives, either to find out regions containing certain body structures or to extract the contours of body structures. For the first objective, segmentation is conducted based on some regional similarity criteria, such as intensity, gradient, texture and so on. ROIs are normally treated as foreground regions R_f and the remainings are treated as background regions R_b. The problem formulation under this objective is modified accordingly. The problem is to find region R_f and R_b, such that

$$R_f \cup R_b = I, \quad R_f \cap R_b = \emptyset. \tag{1.1.2}$$

For the second objective, segmentation is conducted based on some discontinuity criteria, such as edges. The problem is to find a set of points $C = \{c_i\}$, which tightly enclose the ROI.

Figure 1.1: X-ray image. Some parts of the bones are overlapped.

1.1.2 Overview of Main Approaches

Existing medical image segmentation approaches can be roughly categorized into manual segmentation, semi-automatic segmentation and automatic segmentation.

For the purpose of accuracy, medical image segmentation is traditionally done manually, *i.e.*, the ROIs are delineated by some exports such as experienced radiologists and doctors. However, manual segmentation method has at least four disadvantages. Firstly, it is quite time-consuming. Segmentation of a series of 1500-2000 transverse images of 512×512 pixels usually takes two to four hours [41]. Manual contouring of multiple axial images is also laborious. Secondly, manual segmentation is subjective. Segmentation by different experts may vary significantly. For example, a disagreement ratio of $14 \sim 22\%$ by experts in brain tumor segmentation was reported in [23]. Thirdly, variability of the same expert under different circumstances may also be large. Fourthly, the brightness and contrast of the display screen will also affect the segmentation process and subsequent analysis [6].

As an alternative, automatic segmentation scheme can partially solve the problems mentioned in manual segmentation. Firstly, it saves a lot of time of experts by by doing segmentation automatically in computers. Secondly, it is less subjective in the sense that given the same parameters, automatic segmentation scheme will obtain the same result regardless of how many times it is executed. Thirdly, it will not be affected by the brightness and contrast of the display screens. However, medical image segmentation, which is usually effortless and swift for the human visual system, is a considerable challenge in computer based automatic program [4]. The difficulties mainly come from four aspects.

Firstly, it is hard to represent domain knowledge in a computer system. The domain knowledge in this case, is the knowledge of human anatomy, which is acquired by the experts through years of systematic training.

Secondly, the shapes of soft tissues inside the human body are not only complex but also highly variable, as shown in Figure 1.2(a) and 1.2(b). The shapes of the stomach in different slices are different.

Thirdly, large variability in medical images may happen between two different people as illustrated in Figure 1.3. We composite two CT images from two different people together by adjusting the transparency of the image in the front.

The fourth difficulty comes from the medical image itself due to the intrinsic properties of the medical imaging systems. Low contrast and missing information can be seen in Figure 1.4(a) and 1.4(b). The pixel intensities in the boundary region are quite similar. It is hard to identify the edges even for humans. A traditional boundary finding algorithm based on gradient information will fail in such cases. In addition, like most of the natural images, noise exists in medical images inevitably. Filters can employed to remove the noise. However, this is done at the cost of losing details of the image.

As a trade off between manual and automatic segmentation, semi-automatic segmentation algorithms which require human interactions, have been proposed. Those interactions include putting a seed in the center of the ROI [2], or roughly initialize a close contour which contains the ROI [22], etc. Semi-automatic segmentation methods, to certain extent, alleviate some labor of experts, and ROIs are directly selected in manual interactions. However, it can not solve the problems in manual segmentation substantially, since the interactions such as initialization may still be quite subjective, and the

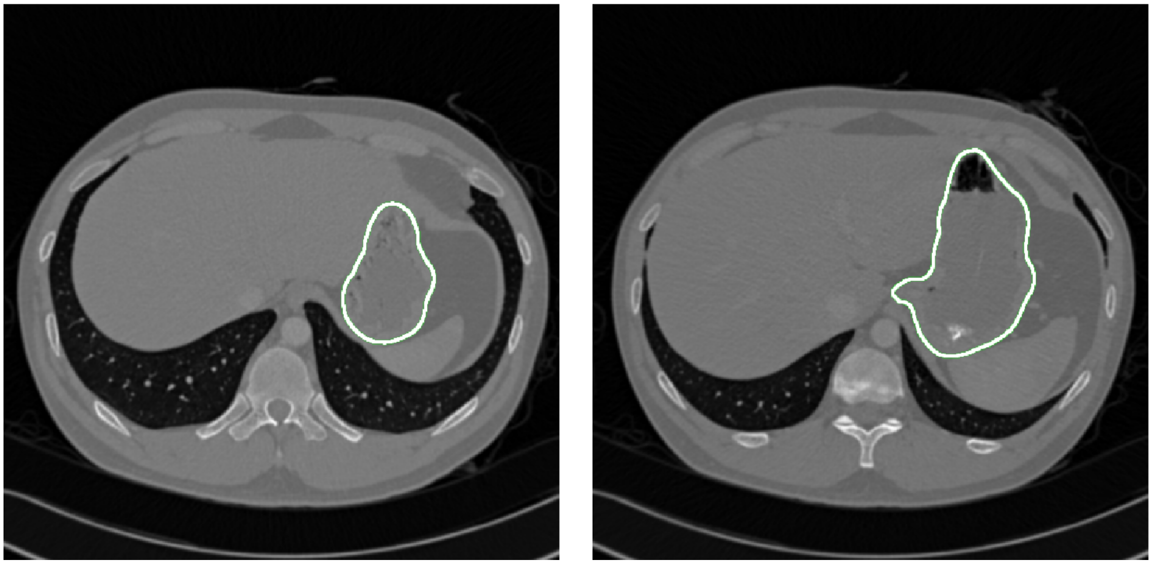

(a) (b)

Figure 1.2: Shape variability of the stomach. (a) and (b) are taken from the same patient. White contours represent the stomach part in (a) and (b), respectively. The Shape of the two contours are quite different. There is even a visible hole inside of the contour in (b).

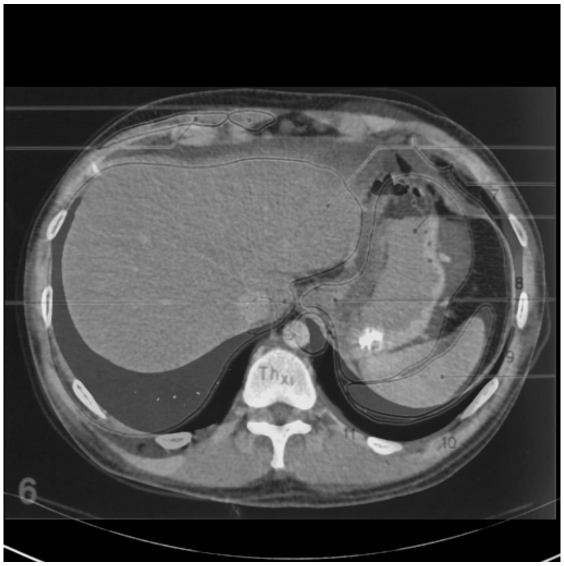

Figure 1.3: Shape variability of soft tissues between different people. Two CT images are composited together.

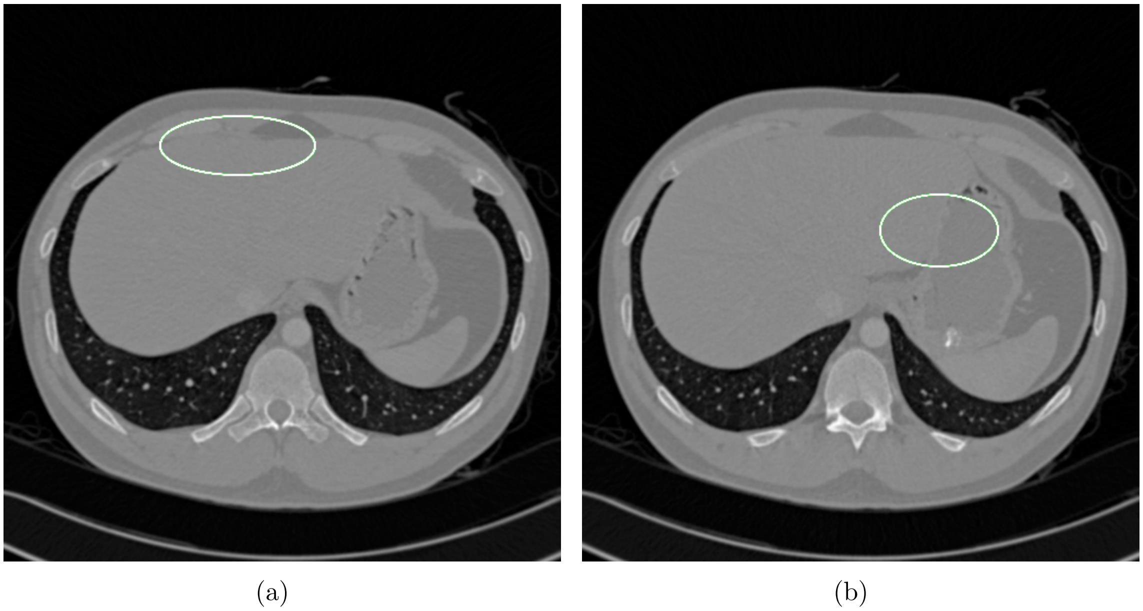

(a) (b)

Figure 1.4: Two CT slices of one patient. The areas circled by white contours are of low contrast, which makes automatic segmentation difficult.

interactions may still be affected by the brightness and contrast of the display screens.

1.2 Organization of the Paper

The rest of this paper is organized as follows. Chapter 2 includes a literature review covering some existing medical image segmentation algorithms and their limitations. Some possible research topics are discussed in Chapter 3. Some preliminary research and the experimental results are described in Chapter 4 and Chapter 5 concludes the paper.

Chapter 2

Literature Review

In this chapter, we review some generic segmentation algorithms as well as some existing medical image segmentation algorithms.

2.1 Generic Segmentation Algorithms

Existing generic segmentation algorithms can be roughly classified into five categories [32].

1. Thresholding
2. Region-Based Segmentation
3. Edge-Based Segmentation
4. Graph-Based Segmentation
5. Classification-Based Segmentation

These methods are described and their pros and cons are analyzed as follows.

2.1.1 Thresholding

Thresholding [36] is one of the basic segmentation techniques. It can roughly be categorized into two, namely *global thresholding* and *local (adaptive) thresholding*, based on the threshold selection criteria.

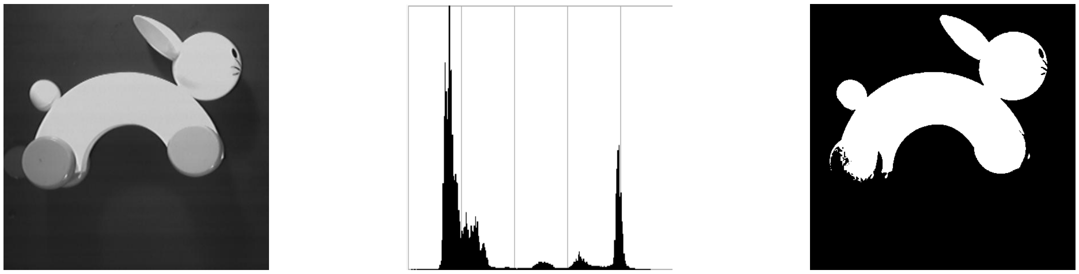

(a) (b) (c)

Figure 2.1: Thresholding of image with bi-modal intensity distribution, (a) original Rabbit image, (b) histogram of Rabbit, and (c) Rabbit after thresholding at $t = 127$.

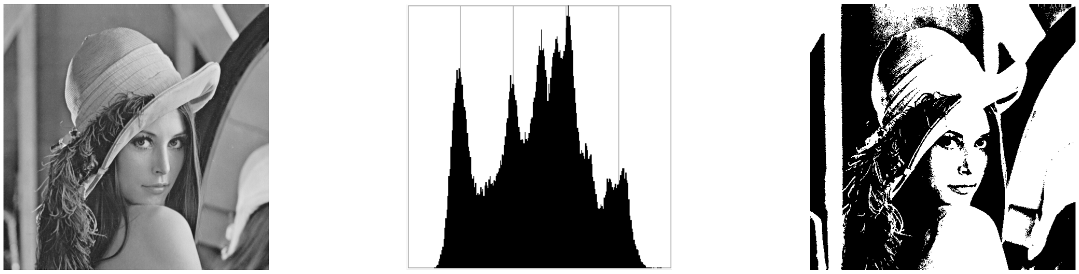

(a) (b) (c)

Figure 2.2: Thresholding of image with multi-modal intensity distribution, (a) original Lena image, (b) histogram of Lena, and (c) Lena after thresholding at $t = 127$.

Given an image I, the global thresholding method tries to find a threshold t, such that pixels with intensity value greater than or equal to t will be "classified" into group 1, and the rest of the pixels into group 2. Binary intensity value will be assigned to pixels in group 1 and 2 accordingly. The computational complexity of this algorithm is very low. However, *global thresholding* assumes that the intensity of the image has a bi-modal distribution. This assumption does not hold for most of the natural images. Examples are shown as follows. The algorithm can perform well on those images with bimodal intensity distribution, as shown in Figure 2.1, while its performance may be poor otherwise, which can be seen in Figure 2.2.

To overcome the shorting-coming mentioned above, several improvements based on global thresholding have been proposed. Histogram shape based thresholding algorithms [7] try to force the multi-modal intensity distributions into smoothed bi-modal distribution. Entropy based thresholding algorithms [33] try to maximize the entropy in the thresholded image.

As an alternative to global thresholding, local thresholding [37] divides an image into multiple sub-images, and select one threshold for each sub-image.

Apart from the bi-modal distribution assumption, thresholding has some other problems. For example, the segmented regions may not correspond to the objects in the original image. The thresholding algorithms do not consider the spatial relationship between pixels. The segmentation result is very sensitive to noise.

2.1.2 Region-based Segmentation

Region-based segmentation algorithms basically consist of *split and merge* algorithm [10], *region growing* algorithm [2, 47] and *watershed* algorithm [5, 34, 31, 27, 18].

Split and Merge

In *split and merge* algorithm, the whole image is initially considered as one region. This region will be split into four quadrants [39], if certain homogeneity criterion is not met. The split process will be repeated recursively until each region contains only homogeneous pixels, as shown in Figure 2.3(a). The algorithm then compares all the regions with their neighboring regions and merge the regions that are similar according to some criteria, as shown in Figure 2.3(b)[1]. The homogeneity criterion is normally based on the intensity value of the pixels. Regions with standard deviation less than a threshold are considered homogeneous. Split and merge algorithm is computationally fast. Its major drawback is its insensitivity to the image semantics.

Region Growing

Region Growing is opposite to the split and merge approach. Traditionally, region growing algorithm begins with selecting n seed pixels. Each seed pixel i is treated as a region A_i, $i \in \{1, 2, ..., n\}$. The algorithm will then try to find some neighboring pixels to those regions and add the pixels to the original regions with similar intensities, thereby growing the regions. An example of region growing segmentation is shown in Figure 2.4[2]. The

---

[1] From http://www.doc.ic.ac.uk/˜dfg/vision/v02.html

[2] From http://www.cse.iitd.ernet.in/˜anup/dip/assgn2/segmentation/

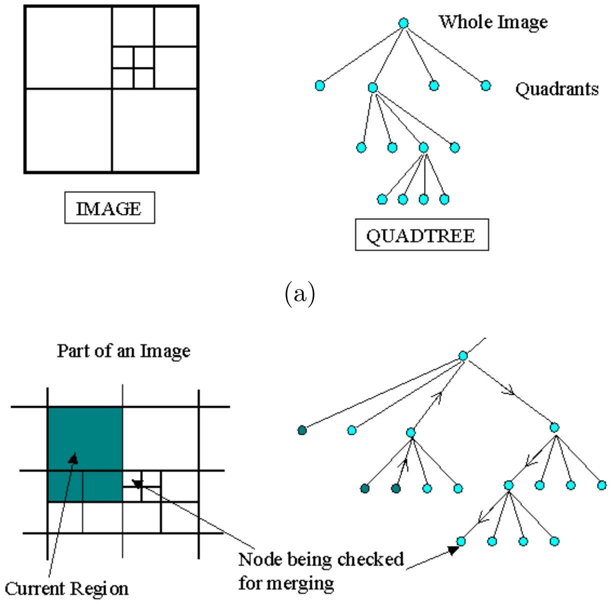

(a)

(b)

Figure 2.3: Split and merge algorithm. (a) is the split process and (b) is the merge process.

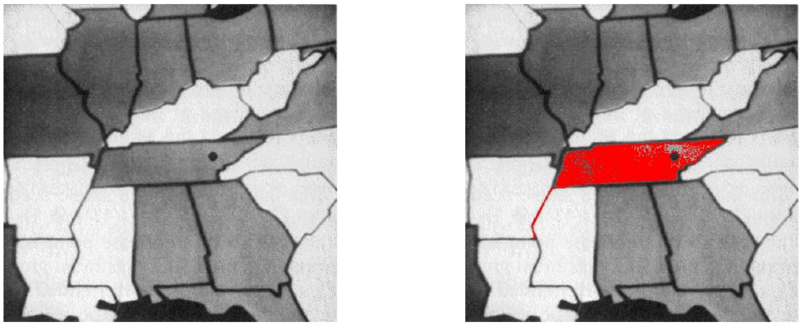

(a) (b)

Figure 2.4: Seeded region growing segmentation. (a) is the source image and (b) is the segmented image.

choice of homogeneity criterion is crucial for the success of this algorithm. A homogeneity criterion proposed by Adams *et al.* [2] is the difference between the pixel intensity value and the mean intensity value of the region,

$$\delta(x) = |g(x) - mean[g(y)]|, \quad y \in A_i \tag{2.1.1}$$

where $g(x)$ is the gray value of the image point x, and x is an unallocated pixel which is adjacent to region A_i. Yu *et al.* proposed another homogeneity criterion in [47]. The idea is to consider the weighted sum of the contrast between the region and the pixel, and the gradient information.

The seed pixel can be selected either manually or by certain automatic procedures. *Converging Square* algorithm [28] was proposed in [2] to automatically find the seed. Converging Square algorithm, as shown in Figure 2.5, divides a square image of size $n \times n$ into four $(n-1) \times (n-1)$ square images, and choose the square image with the maximum intensity density for the next division cycle. This process continues recursively until a seed point is found.

Region growing algorithms are fast, but may produce undesired "segments" if the images contain much noise. It is also inappropriate for highly textured images.

Watershed

The watershed algorithm [5] is another region-based image segmentation approach. It was originally proposed by Beucher *et al.* It is a popular segmentation method coming from

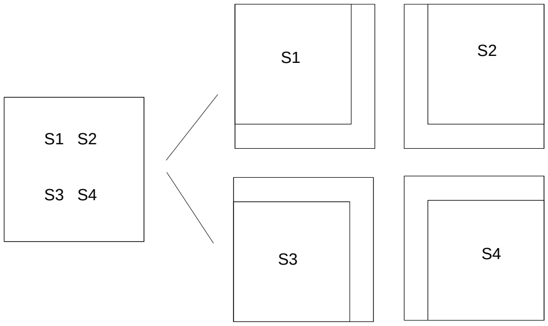

Figure 2.5: Converging Square. Each square of width k is divided into 4 overlapping squares of width $k-1$.

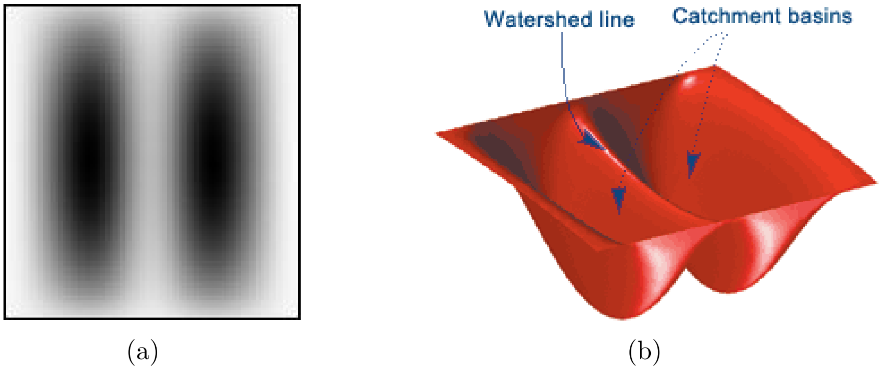

(a) (b)

Figure 2.6: Watershed algorithm model. (a) is the source image and (b) is the topological illustration. Regions with low intensities in (a) correspond to the catchment basins in (b), and the region between is the watershed line.

the field of mathematical morphology. According to Serra [34], the watershed algorithm can be intuitively thought as a landscape or topographic relief which is flooded by water, and watersheds are the dividing lines of the domains of attraction of rain falling over the region. The height of each point represents its intensity value, as can be seen in Figure 2.6[3]. The input of the the watershed transform, generally, is the gradient of the original image, so that the catchment basin boundaries are located at high gradient points [31].

The watershed transform has good properties that make it useful for many different image segmentation applications: it is simple and intuitive. It can also be parallelized [31], and always produces a complete division of the image. However, it has several major drawbacks. It can result in over-segmentation, *i.e.,* the segmentation result contains

---

[3] From http://www.mathworks.com/company/newsletters/news_notes/win02/watershed.html

(a) (b)

Figure 2.7: Over-segmentation of watershed algorithm, (a) source image and (b) over-segmented image.

many small regions. The effect of over-segmentation can be seen in Figure 2.7[4]. It is also sensitivity to noise. Moreover, watershed algorithm is poor at detecting thin structures and structures with low signal-to-noise ratio [18].

To improve the algorithm, Najman *et al.* proposed to use morphological operations to reduce over-segmentation [27]. Grau *et al.* [18] encoded prior information into the algorithm. Part of its cost function is changed from the gradient between two pixels to the difference of posterior probabilities of two pixels given their intensity as prior information. The authors assume normal distributions for the objects in the image, so that Markov Random Fields (MRF) model can be deployed.

2.1.3 Edge-based Segmentation

Edge-based segmentation algorithms use edge detectors to find edges in the image.

Traditional *Sobel* edge detector [17] contains a pair of 3 by 3 convolution kernels, as shown in Figure 2.8. It calculates the first order derivatives (gradient) along x and y directions of the original 2-D image. The magnitude of the resulting edge is the gradient of the original image.

Instead of computing first order derivatives, the *Laplacian* computes the second order derivatives of the image. Usually, the Laplacian is not used directly on the original image, since it is sensitive to noise. It is often combined with a Gaussian smoothing kernel, which

---

[4] From http://www.icaen.uiowa.edu/~dip/LECTURE/Segmentation3.html

-1	0	+1
-2	0	+2
-1	0	+1

(a)

+1	+2	+1
0	0	0
-1	-2	-1

(b)

Figure 2.8: Sobel kernel pair, (a) kernel x and (b) kernel y.

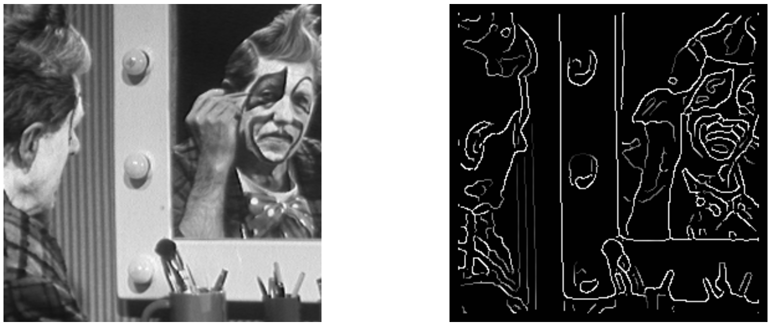

(a) (b)

Figure 2.9: Canny edge detection result, (a) source image and (b) edge map obtained by Canny edge detector.

is referred to as the *Laplacian of Gaussian* function.

However, edges found by these operators are normally disjoint, and cannot completely represent the boundary of an object. Canny edge detector [8] uses a double-thresholding technique. A higher threshold t_1 is used to detect edges with strict criterion, and a lower threshold t_2 is to generate a map which can help to link the edges detected in the former step. An example of Canny edge detection result is shown in Figure 2.9.

Edge-based image segmentation algorithms are usually with low computational complexity, but they tend to find edges which are irrelevant to the object, and the contours of the object are often disjointed, *i.e.* closed and connected regions are less likely to be obtained by edge-based algorithms.

2.1.4 Graph-based Segmentation

Graph-based approach is relatively new in the area of image segmentation. The common theme underlying this approach is the formation of a weighted graph, where each vertex corresponds to an image pixel or region and each edge is weighted with respect to some measure. A graph $\mathbf{G} = (\mathbf{V}, \mathbf{E})$ can be partitioned into two disjoint sets, namely A and B, where $A \cup B = V$ and $A \cap B = \emptyset$. Graph-based algorithms try to minimize certain cost functions, such as a *cut*,

$$cut(A, B) = \sum_{u \in A, v \in B} w(u, v). \tag{2.1.2}$$

Wu *et al.* proposed the *minimum cut* in their workspace [45]. A graph is partitioned into k sub-graphs such that the maximum cut across the subgroups is minimized. However, based on this cutting criterion, their algorithm tend to cut small sets of isolated nodes in the graph, since the value of Eqn. 2.1.2 is, to some extent, proportional to the size of the sub-graph. To avoid this bias, Shi *et al.* [38] proposed the *normalized cut* with a new cost function *Ncut*,

$$Ncut(A, B) = \frac{cut(A, B)}{assoc(A, V)} + \frac{cut(A, B)}{assoc(B, V)} \tag{2.1.3}$$

where $assoc(X, V) = \sum_{u \in X, t \in V} w(u, t)$ is the total connection from nodes in X to all nodes in the graph. In [43], Wang *et al.* further improved the graph cut algorithm, and proposed a new cost function for general image segmentation, namely *Ratio Cut*. This scheme is to find the minimal ratio of the corresponding sums of two different weights associated with edges along the cut boundary in an undirected graph.

$$Rcut(A, B) = \frac{c_1(A, B)}{c_2(A, B)} \tag{2.1.4}$$

where $c_1(A, B)$ is the first boundary cost that stands for the homogeneity of A and B, $c_2(A, B)$ is the second boundary cost that stands for the number of edges between A and B. A polynomial-time algorithm is also proposed.

Compared to region-based segmentation algorithms, graph-based segmentation algorithms tend to find the global optimal solutions, while region-based algorithms are based on greedy search. Since graph-based algorithms try to find the global optimum, it is computationally expensive. The Over segmentation is also one of the problems.

2.1.5 Classification-based Segmentation

Ren *et al.* proposed to train a classifier to classify “good segmentation” and “bad segmentation” [30]. The criteria used for the classification include texture similarity, brightness similarity, contour energy, curvilinear continuity, etc. A preprocessing step which groups pixels into “superpixels” is used to reduce the dimension of the image. This step is actually done by applying the normalized cut algorithm [38]. Human segmented natural images are used as positive examples, while negative examples are constructed by randomly matching human segmentations and images.

Fuzzy reasoning methods are proposed to detect the cardiac boundary automatically [14, 6]. The Laplacian-of-Gaussian approach is employed to obtain the zero-crossing area of the original image. From those zero-crossing areas, fuzzy set is used to describe the direction and transition of intensity values. Fuzzy rules come from global knowledge presented by medical experts. A rough boundary region is obtained after fuzzy reasoning, where a search operation is followed to get the boundary.

Toulson *et al.* proposed to use a Back Propagation neural network in image segmentation [42]. The neural network is trained on the set of manual segmented samples. Therefore, contextual rules can be learned and spatial consistency of the segmentation can be improved. Also, expert knowledge can be incorporated into the segmentation where boundaries may not be justifiable based on intensity information.

Classification-based segmentation algorithm requires training. The learning parameters are usually set in a trail and error way, which is subjective. The accuracy of this algorithm largely depends on the selected training samples. Also, classification-based segmentation algorithm is more tedious to use.

2.1.6 Comparison

A comparison of generic segmentation algorithms mentioned above is made according to the information used, performance, computational complexity, whether they are sensitive to noise, whether manual initialization is required, whether training is required and whether they are easy to use. The results are shown in Table 2.1. Thresholding algorithm uses the information based on single pixel, while other algorithms mainly use

Table 2.1: Comparison of generic segmentation algorithms.

	Thresholding	Region-based	Edge-based	Graph-based	Classification-based
Information	pixel	patch	patch	patch	patch
Performance	depend on intensity distribution	over segmentation	disjoint edges	over segmentation	depend on training set
Complexity	$O(n)$	$O(n)$	$O(n)$	$O(n \log n)$	$O(n)$
Manual Init	no	yes	no	no	no
Training	no	no	no	no	yes
Easy to Use	yes	yes	yes	yes	no

information based on a local pixel patch. The performance of thresholding algorithm is depend on the intensity distribution of images. Edge-based algorithm tend to produce disjoint edges. In addition, all the algorithms have over-segmentation tendency. The computational complexities of thresholding, region-based and edge-based algorithms are roughly linear, while those of the other two algorithms are higher. All the algorithms are sensitive to noise. Region-based algorithm usually requires manual initialization. Classification-based algorithm requires training. Most of the algorithms are easy to use except classification-based algorithm.

The boundaries found by generic segmentation algorithms such as edge detectors do not necessarily correspond to the boundaries of objects. The limitations of edge detectors are due to their reliance on the information coming from a local neighborhood of pixels in the original image. This ignores both model-based information and higher order organization of the image. However, Using models tends to result in a more consistent solution overall.

2.2 Widely Used Segmentation Algorithms for Medical Images

In this section, we review some specific segmentation algorithms that are widely used for medical images, including the active contour model, level set, active shape model, other free-form deformable model and atlas-based segmentation algorithm.

2.2.1 Active Contour Models

The *Snake* [22] model was first proposed by Kass *et al.*. The basic snake model represents a contour $\mathbf{v}$ parametrically as $\mathbf{v} = \mathbf{v}(s) = (x(s), y(s))$, $s \in [0, 1]$. It is a controlled continuity spline which can deform to match any shape, under the influence of image forces and external constraint forces. The internal spline forces serve to impose a piecewise smoothness constraint. The image features attract the snake to the salient image features such as lines, edges and terminations. The total energy of the snake can be written as

$$E^*_{snake} = \int_0^1 E_{snake}(\mathbf{v}(s)) = \int_0^1 [E_{int}(\mathbf{v}(s)) + E_{image}(\mathbf{v}(s)) + E_{con}(\mathbf{v}(s))]\, ds \tag{2.2.1}$$

where E_{int} represents the internal energy of the spline, E_{image} represents the image forces, and E_{con} represents the external constraint forces. The internal energy can be written as

$$E_{int} = (\alpha(s)|\mathbf{v}_s(s)|^2 + \beta(s)|\mathbf{v}_{ss}s|^2)/2 \tag{2.2.2}$$

The first order term represents the stretching force of the snake while the second order term represents its bending force. The image energy can be written as

$$E_{image} = w_{line}E_{line} + w_{edge}E_{edge} + w_{term}E_{term} \tag{2.2.3}$$

The external constraint energy E_{con} has many forms, such as spring energy and repulsion force.

The snake algorithm will iteratively deform the model and try to find the configuration with minimum total energy E^*_{snake}, which hopefully corresponds to the best fit.

Atkins *et al.* [3] used the active contour for brain segmentation. The input images are first smoothed, and an initial mask that determines the brain boundary. Final segmentation is then performed by the snake model.

The values of α and β in the original snake model are chosen subjectively. Gao *et al.* [15] proposed a solution to specify their values in automatic extraction of the liver boundary, several preprocessing steps are first performed on the original images. The preprocessing steps include i) thresholding to discard pixels whose gray levels are out of the range for the liver; ii) remove the texture and noise; iii) extract and link the edges by some edge linker; iv) segmentation using a modified version of split-and-merge; v) guess the initial liver contour. After the preprocessing, the liver boundary is refined by snake

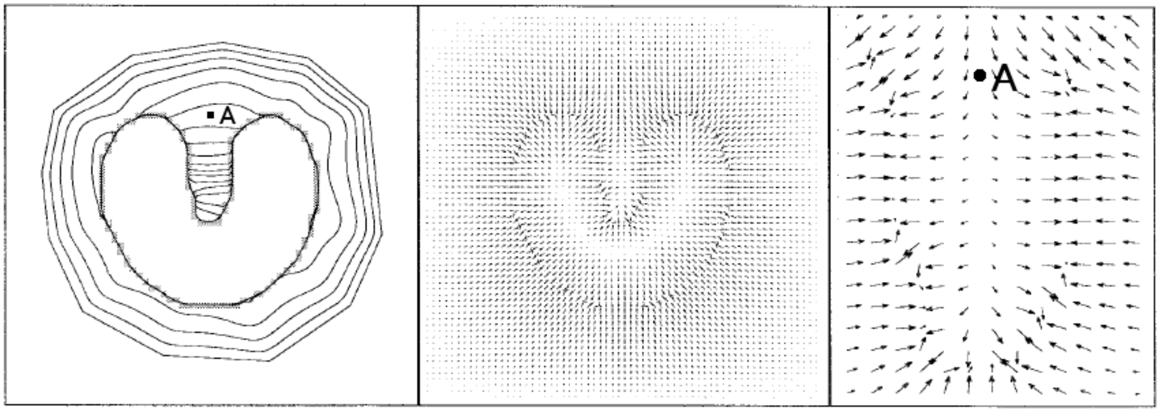

Figure 2.10: Gradient vector flow [46]. Left: deformation of snake with GVF forces. Middle: GVF external forces. Right: close-up within the boundary concavity.

algorithm. In the internal energy term E_{int}, the value of α is proportional to the distance of adjacent control points, while β_i is inversely proportional to the curvature value.

Snake is a good model for many applications, including edge detection, shape modeling, segmentation and motion tracking. However, it has some intrinsic problems. Firstly, the result of snake algorithm is sensitive to the initial configuration of the contour. Secondly, it cannot converge well to concave features. To solve theses two problems, a new external force, *gradient vector flow* (GVF), was proposed by Xu *et al.* [46]. Define $\mathbf{v}(x, y) = [u(x, y), v(x, y)]$, and the energy function in GVF is

$$\varepsilon = \iint \mu(u_x^2 + u_y^2 + v_x^2 + v_y^2) + |\nabla f|^2 |\mathbf{v} - \nabla f|^2 \, dx \, dy \tag{2.2.4}$$

where ∇f is the gradient of the edge map $f(x, y)$, which is derived from the original image. μ is a regularization parameter governing the trade-off between the first term and the second term. When $|\nabla f|$ is small, the energy is dominated by the first term, yielding a slowly varying field. When $|\nabla f|$ is large the second term dominates the equation, which is minimized by setting $\mathbf{v} = \nabla f$. As shown in Figure 2.10, at point A, there is no edge value. The original snake algorithm cannot “pull” the contour into the concavity of the U-shape. GVF can propagate the edge forces outward, and at point A, there is still some external forces that can “pull” the contour into the concavity.

GVF is less sensitive to the initial position of the contour than the original snake model. However, it is still requires a “good” initialization. In addition, it is also sensitive to noise, which may attract the snake to undesired locations.

2.2.2 Level Set

Snake-based deformable model cannot handle applications which require topology changes. Sethian proposed a *level set* [35] approach to deal with this problem in one higher dimensional space. Let Γ be an initial closed curve in 2-D. Define a 3-D level set function $\phi(\mathbf{x}(t), t)$, where $\mathbf{x}(t)$ is the path of a point on the propagating front.

$$\Gamma = \phi(\mathbf{x}(0), 0) \tag{2.2.5}$$

An example 3-D level set function is shown in Figure 2.11. Moving ϕ along t can yield 2-D contour at different time t, and the solution of equation $\phi = 0$ is the desired contour.. The change of ϕ over time t is derived as follows.

Based on the chain rule,

$$\phi_t + \sum_{i=1}^{N} \phi_{x_i} x_{i_t} = 0 \tag{2.2.6}$$

where x_i is the ith component of $\mathbf{x}$. The summation term is

$$\sum_{i=1}^{N} \phi_{x_i} x_{i_t} = (\phi_{x_1}, \phi_{x_2}, \ldots, \phi_{x_N}) \cdot (x_{1_t}, x_{2_t}, \ldots, x_{N_t}) = |\nabla\phi||\mathbf{x}(t)| cos(\widehat{\nabla\phi, \mathbf{x}(t)}) = F(\mathbf{x}(t))|\nabla\phi| \tag{2.2.7}$$

So, a Hamilton-Jacobi “type” equation

$$\phi_t + F|\nabla\phi| = 0 \tag{2.2.8}$$

can be obtained, where F is the force which gives the speed of Γ in its normal direction.

The major advantage of the level set approach is that the level set function ϕ remains a function while the hyper-surface may change topology, break, merge and form sharp corners [24]. However, it generally cannot maintain shape information.

2.2.3 Active Shape Model (ASM)

The objects in medical images, such as organs, cells, and other biological structures, are expected to have a tendency towards some average shape with a continuum of possibilities near that average shape. This tendency can be taken advantage of by its expression in an appropriately designed shape model [40].

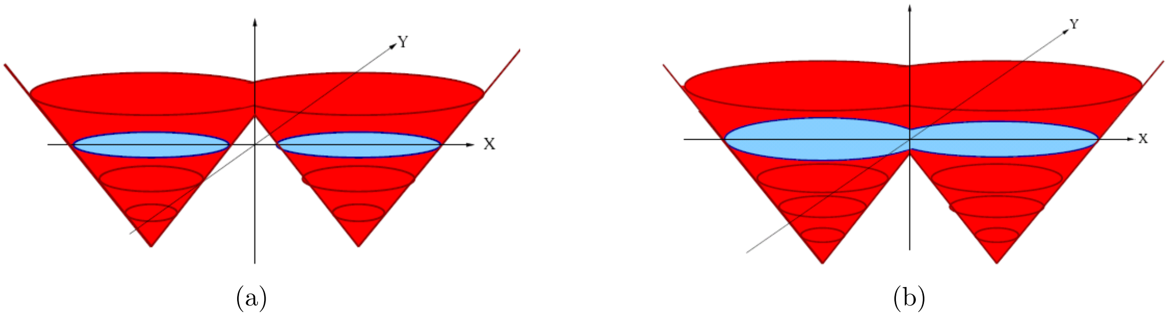

(a) (b)

Figure 2.11: Level set. (a) Two separate initial fronts (b) The interface topology has changed, yielding a single curve as the zero level set.

Cootes *et al.* [12] proposed to use *Active Shape Models*, a statistical model, to locate structures in medical images. Given the training images, a covariance matrix is computed first. The algorithm then applies Principal Component Analysis (PCA) to identify the eigen-shapes. An arbitrary shape can be represented by the linear combination of these shapes with different coefficients. Therefore, the model can be deformed by changing these coefficients. An initial guess can be obtained by Hill's algorithm [20]. Then an optimization algorithm such as gradient descent can be used to find the optimal solution.

Based on Cootes' model, Wang *et al.* [44] proposed to use smoothness covariance matrix, instead of the original covariance matrix to remove part of the dependency between points. Thus the shape can vary more freely. A Bayesian formulation based on prior knowledge and the edge information of the input image is employed to bias the searching process in a certain range for the object boundary. Similar work was done by Gleason *et al.* [16] in detecting polycystic kidney disease in CT images.

One of the disadvantages of this algorithm is that it require a lot of training samples. Also, eigen space with small number of eigen shapes may not generate the desired shape, while eigen space with large number of eigen shapes may incur high complexity in finding the optimal solution.

2.2.4 Other Free-form Deformable Models

Some other free-form deformable models are also proposed in the literature, which can be categorized into *parametric models* [40, 21, 25] and *non-parametric models* [19].

Parametric models have the advantage of capturing the overall shape in a small number of parameters. Therefore the optimization of a match measure between data and model can occur in a low dimensional space.

Staib *et al.* [40] proposed a parametric model based on elliptic Fourier decomposition to enhance the segmentation of natural objects found in biomedical images. The boundary template is obtained by manual segmentation of a set of exemplar images. An object function which is a measure of fit between the boundary model and object boundary is maximized using maximum *a posteriori* method.

Mattes *et al.* [25] proposed to use B-splines in the local deformation because of their computational efficiency. Metaxas *et al.* [26] proposed elastically adaptive deformable models based on superellipsoid.

However, parametric models may not have enough parameters to represent the details of the shape such as high curvature part.

Non-parametric models use all the pixels on the contour, which can model arbitrary shapes. Grzeszczuk *et al.* [19] proposed some stochastical deformation algorithms, namely "Raindrop" and "Bike Trail", which can deform the contour stochastically. For each configuration of the contour, its energy is computed. To find the global minimum energy of the contour, simulated annealing is introduced. However, the search space for optimal solution is incredibly large.

2.2.5 Atlas-Based Segmentation

Atlas-based segmentation has become a standard paradigm for exploiting prior knowledge in medical image segmentation [13]. The idea is to construct an atlas based on some prior information, and use this atlas to aid the segmentation of other similar structures in the low contrast medical images. The prior information can be the contour or surface of an object [11, 1, 29] or some density map [41]. Generally, the process of atlas-based segmentation is that the atlas is first placed near to the desired contour by linear or non-linear global transformation, and then registered to the input images by local transformation according to some measure of fit.

Broadly speaking, the construction of the atlas is based on two kinds of prior information, either a single object or multiple objects.

For atlas construction based on a single object, the object itself is treated as the atlas. However, such atlas may have several problems. Firstly, the selection of a single object as the atlas is arbitrary, and the selected object may not be a typical one. Secondly, the use of atlas based on a single object does not contain any information of variability, so it is impossible to determine whether a transformed shape is an acceptable shape.

To solve these problems, *probabilistic atlas* is proposed in [11, 1, 29], which is the spatial distribution of probabilities that a pixel belongs to one organ [29]. The distribution of probabilities can be obtained from a set of sample images as the prior information. The active shape model [12], is actually a probabilistic atlas. The disadvantage of probabilistic atlas is that it requires a lot of training samples to model the probability. Moreover, the probabilistic atlas can be either a uni-model or multi-model. The uni-model has the limitation to model complex probability distribution; while the multi-model itself is very complicated.

2.2.6 Comparison

As shown in Table 2.2, a comparison of different medical image segmentation algorithms is also conducted similar to that in Section 2.1.6. Most of the algorithms are based on curve information, while atlas-based algorithms also employ global image information. The computational complexity of all the algorithms are high. Apart from level set algorithm, they can not handle topology change generally. They are all sensitive to noise, while ASM and atlas-based algorithms may be affected less by noise. They are all sensitive to the initial configuration of the contours. Generally, all the algorithms require manual initialization, while atlas-based segmentation algorithm requires less manual initialization work. ASM and atlas-based algorithms also require training.

2.3 Evaluation

To evaluate medical image segmentation algorithms, the only information available is boundaries outlined by multiple expert observers, the average of which is used as the ground truth data.

Table 2.2: Comparison between specific segmentation algorithms for medical images.

	Snake	GVF	Level Set	ASM	Other Free-form		Atlas
					Parametric	Non-parametric	
Information	Curve						Global
Handle Topology Change	no	no	yes	no	no	no	no
Sensitive to Noise	yes	yes	yes	relatively low	yes	yes	relatively low
Training	no	no	no	yes	no	no	yes

Similarity Index is first proposed by Zijdenbos *et al.* [48]. The similarity of two segmentations A_1 and A_2 can be represented by

$$S = 2\frac{|A_1 \cap A_2|}{|A_1| + |A_2|} \tag{2.3.1}$$

This similarity index is sensitive to both size and location of the segmentations.

Chalana *et al.* [9] proposed a methodology to evaluate medical image segmentation algorithms against the ground truth. Error metric used in Chalana's methodology is the Distance to the Closest Point (DCP). Let $A = \{a_1, a_2, ..., a_m\}$ and $B = \{b_1, b_2, ..., b_m\}$ represent two curves, where a_i and b_i are ordered pair of x and y coordinates of a point on the curve. DCP for a_i to the curve B is

$$d(a_i, B) = \min_j \parallel b_j - a_i \parallel \tag{2.3.2}$$

Chapter 3

Possible Research Topics

Based on the literature review in Chapter 2, atlas-based approach is the most prosperous one in medical image segmentation. Two possible research topics on atlas-based approach are proposed here.

3.1 New Form of Atlas-based Segmentation

Atlas-based algorithm, especially probabilistic atlas, is a powerful approach in medical image segmentation. It can not only provide an average model given the training sample, but also provide the distribution of the model, which can limit the program in a certain range to find the optimal solution. However, it is such limitation that will constrain atlas-based algorithm itself. Therefore atlas-based algorithm generally can not handle large shape changes of the body parts caused by some diseases, which are not be represented by the training sample. So one possible research topic is to combine the probabilistic approach with other approaches such as snake and level set, etc., which yield more flexible deformation while still under the guidance of the atlas.

3.2 Atlas Building

Atlas-based algorithm is based on the deformation of the atlas. The quality of atlas will definitely affect the performance of the algorithm. So a good atlas is required. Most existing literatures put their weight on explaining how the atlas can be used, rather than how to build an atlas. This can be a problem when multiple prior training samples are available. There are some papers which propose to calculate the mean and the covariance of the training samples as the atlas. However, if the training samples themselves contain complex topology and large variances, how to find a mathematically "sound" mean is a big problem. Also, the atlas is generally obtained by manual segmentation of large number of sample images, which has all the disadvantages of manual segmentation mentioned in Chapter 1, such as quite time-consuming, subjective, inter- and intra-expert variability, etc. So, the second possible research topic is to find an good learning approach to build the atlas from a set of training samples, and with less manual work.

Chapter 4

Preliminary Work

In this chapter, we describe some preliminary work which has been done using atlas-based segmentation. The objective is to implement a robust and automated method of registering 2D deformable models to the 2D CT images of human body parts. The body parts included in this work are liver, stomach, spleen and thoracic aorta.

4.1 Problem Definition

The problem of automatic segmentation of the soft tissues in CT images can be formulated as a problem to deform the reference model contour and register it to the edges of corresponding soft tissues in the target CT images.

- The inputs of the problem: $M = \{p_i\}$ is the control points located on the reference model contour, S is the intensity difference distribution along the normal of contour represented by p_i in the reference image, S' is the intensity difference distribution along the normal of the deformed model contour represented by $M' = \{p'_i\}$, $C = \{q_j\}$ denotes the set of edge points in the image, which include edge points along the contour of the soft tissue and possibly other noise points, such as edge points along the contour of other soft tissues, noise edges, etc. Also, some points on the soft tissue contour in the image may not be in C because they are not prominent edge points.
- The output of the problem: $M' = \{p'_i\}$ is the extracted contour on the target image,

which is represented by a deformed version of M.

We assume that the input CT images always contain the full view of cross section image of the abdomen, and the anatomical structures between different CT images do not differ too much. We also assume that the background of the input CT images (outside the body contour) is mainly black.

The objective of the registration problem is to find the deformation $D : \mathbb{R}^2 \rightarrow \mathbb{R}^2$, affine transformation $T : \mathbb{R}^2 \rightarrow \mathbb{R}^2$ and correspondence function $f : \mathbb{R}^2 \rightarrow \mathbb{R}^2$ such that the total error E can be minimized.

$$E = \frac{1}{|m|} \left[\sum_{p_i \in m} ||D(T(p_i)) - f(p_i)||^2 + \alpha \sum_{p_i \in m} ||S(p_i) - S'(D(T(p_i)))||^2 \right] \tag{4.1.1}$$

$m \subseteq M \ s.t. \ ||D(T(p_i)) - f(p_i)|| < \Gamma$, for an appropriate predefined threshold Γ, and α is a constant.

4.2 Algorithm

The main idea is to transform the model contours and make them close to the real contours in the input CT images. These initial contours are then treated as an input to the standard GVF snake program and refined by the program.

The transformation is taken in two steps, namely global transformation and local transformation.

4.2.1 Global Transformation

In global transformation, we use a contour tracing algorithm to get the outer body contour in the target image, which is part of M. We perform 2D-2D registration with unknown correspondence between reference body contour and input body contour using *Iterative Closest Point* algorithm. After the registration, its transformation matrix can be obtained by solving a set of over-constrained linear equations. This transformation matrix is then applied to the contours of inner body parts. The contours obtained after global transformation are $M_1 = \{M_{11}, M_{12}, M_{13}, M_{14}\}$, where M_{11}, M_{12}, M_{13}, and M_{14} are

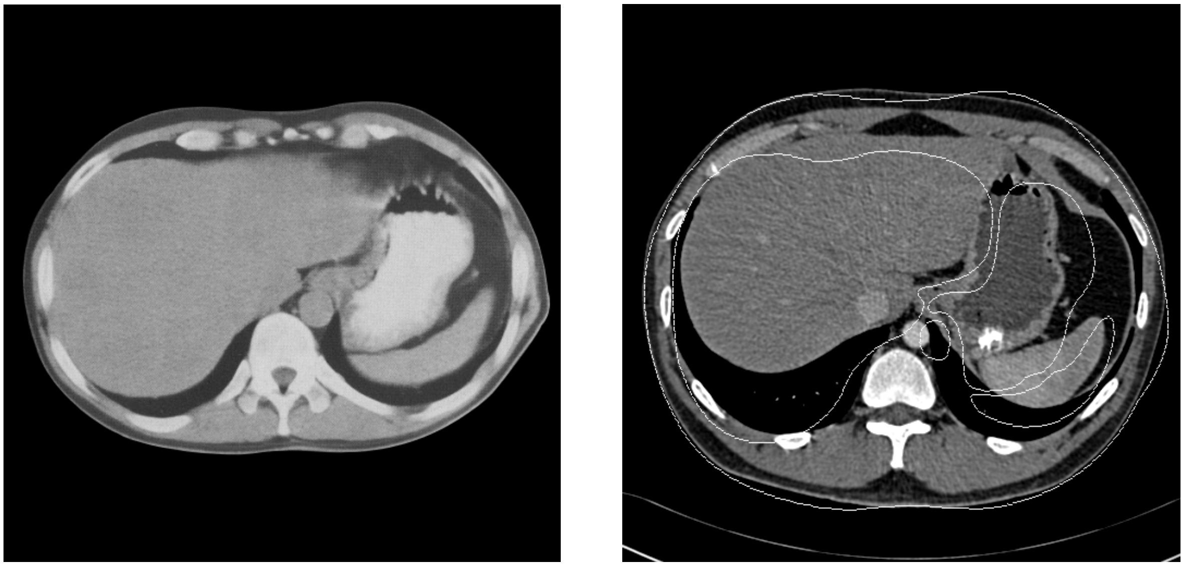

(a) (b)

Figure 4.1: Global transformation. (a) The model image. (b) The target image. The white contour is the model contour after global transformation.

corresponding to the contours of liver, stomach, spleen and thoracic aorta, respectively. The results of global transformation are shown in Figure 4.1.

Global transformation, however, can only help to roughly place those contours, which is normally far from the desired contours. A further step, local transformation, is used to solve this problem.

4.2.2 Local Transformation

Compared to the global transformation mentioned above, local transformation is to transform the body parts individually. In this work. we categorized the four body parts into two groups based on their sizes and conduct different local transformation strategies accordingly.

The first group includes liver, stomach and spleen, which are relatively large objects in the input images. For these objects, we assume that the centroid of the contour after global transformation is inside of the real body parts in the input images. For this group, the idea is to iteratively transform the model contours and make them closer and closer to the real body parts contours in the input images. To achieve this, several steps are

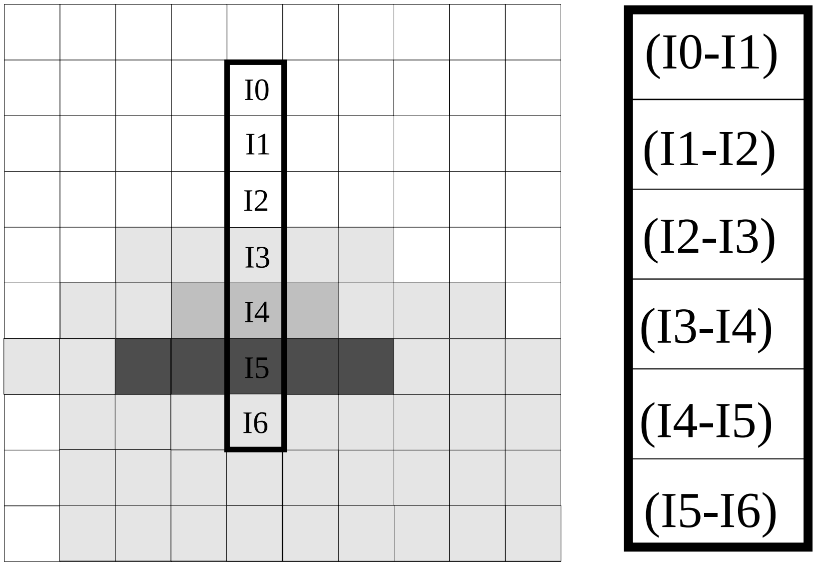

(a) (b)

Figure 4.2: Intensity difference distribution. (a) $I_0, I_1, I_2, I_3, I_4, I_5$ and I_6 are intensity values along the normal of the contour. (b) The intensity difference distribution is given by substraction of the intensity values of neighboring pixels.

employed.

1. Move the model contour points $M_{1i} = \{p_{ij}\}(i = 1, 2, 3, 4)$ along the normal of the contour within some search range to find a list of candidate edge points L_{ij} in the edge map of the input image.

2. Compute the intensity difference of the neighboring pixels along the normal of the model contour in the reference image with the contour point p_{ij} at the center. The intensity difference of the pixels gives intensity difference distribution (IDD). A sample IDD with length 6 is shown in Figure 4.2.

3. For each point in L_{ij}, compute IDD along the contour with the corresponding point of p_i in the input image at the center.

4. Compute the Euclidean distance between the IDD in the image and the IDD in the input image of each candidate points in L_{ij}, and select the point q_{ij} with the minimum distance in L_{ij}.

5. A verification step is also carried out by shooting rays from the centroid to the

selected points q_{ij}. If the number of "black" or "white" points along the path exceeds some threshold, the points are then discarded (the color of the body parts is typically "gray" in CT images).

6. With the model contour points p_{ij} and their correspondence points q_{ij} selected in the previous steps, a transformation matrix can be obtained by solving a set of over-constrained linear equations. This matrix is used to transform the model contour.
7. The square of Euclidean distances between transformed model contour points and their correspondence points are computed and summed up as the error e_i.

$$e_i = \sum_j ||p_{ij} - q_{ij}||^2 \tag{4.2.1}$$

8. Iteratively perform the previous steps until the error e_i is small enough.

The second group includes thoracic aorta, which is significantly smaller then the body parts in the first group. Therefore, the assumption we made for the first group does not hold for it, which can be easily seen in Figure 4.3. Since the shapes of the thoracic aorta in the different CT images are roughly circular with similar size, a circle with similar size is used as the model contour. The center of the model circle is placed at the centroid of the model thoracic aorta contour obtained after global transformation. The circle is moved in a search window in the edge map and the Euclidean distance error between model circle and edge points in the input images is computed. The position with the minimum error is selected to place the circle.

The model contours after local transformation are shown in Figure 4.3.

4.2.3 GVF Snake

After all the transformations are done, the transformed model contours are fed into the standard GVF snake program. The snake model is run to iteratively deform the model to refine the model contour to better capture the input object contour.

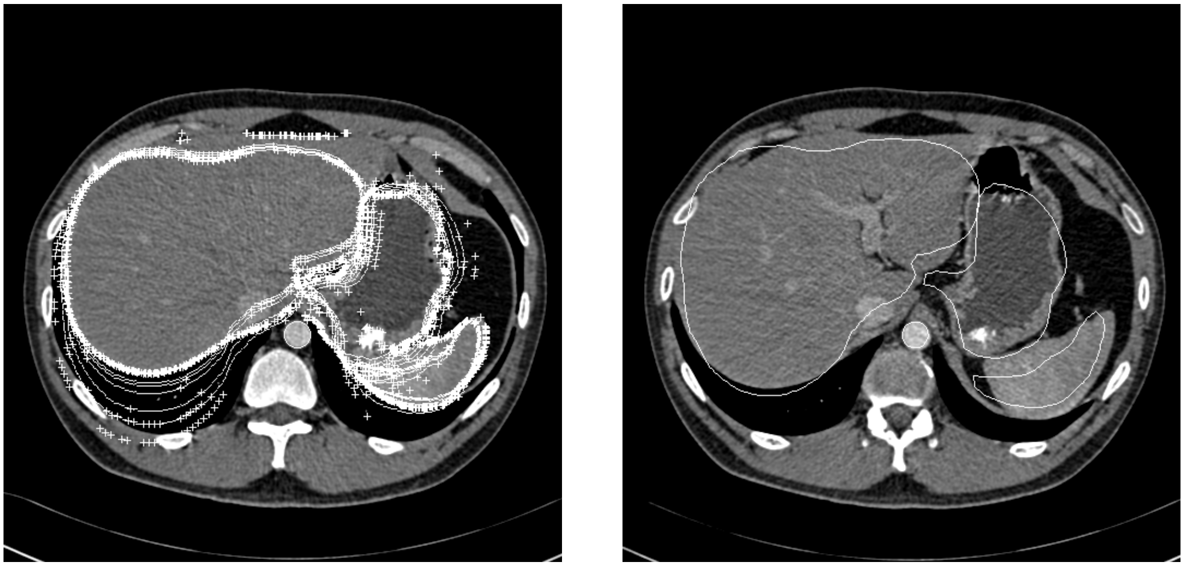

(a) (b)

Figure 4.3: Local transformation. (a) The white contours are iteratively transformed. The white crosses are selected corresponding points in each iteration. (b) The resulting contours of local transformation, which will be fed to GVF snake program for the refinement.

4.3 Results and Discussion

The final segmentation results are shown in Figure 4.4. More segmentation results are shown in Figure 4.5. As a comparison, segmentation result without local transformation is shown in Figure 4.6. The final contours are more or less attracted to the wrong places, which are not desired.

A quantitative evaluation is also conducted. For the five input images given, the four body parts in each images are manually segmented as the "ground truth" data. They are compared with the results generated by the segmentation algorithm. *Similarity Index* proposed by Zijdenbos *et al.* [48] is used to evaluate the algorithm's performance. The results are shown in Table 4.1.

As we may observe, the similarity indices of stomach in the input images are relatively low. The reason is that the proposed algorithm excludes the hollow in the stomach, which is included in the manually segmented stomach. The similarity indices of thoracic aorta in the input images are also lower than liver and spleen, while perceptually, thoracic aorta

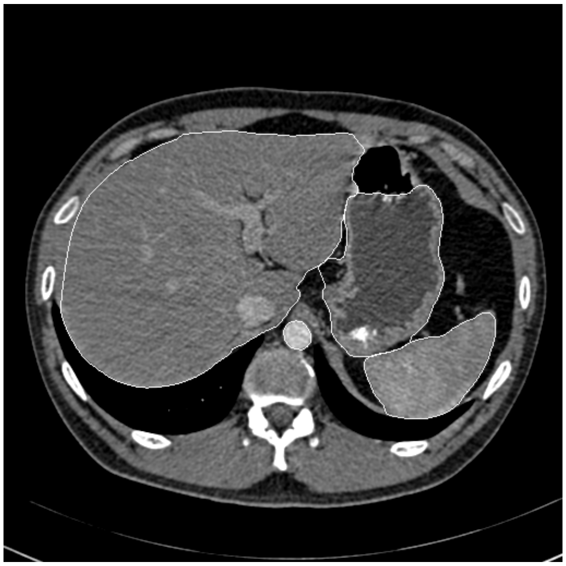

Figure 4.4: Final result of input image 2. The liver, stomach spleen and thoracic aorta are enclosed in white contours.

Table 4.1: Segmentation similarity index.

	Liver	Stomach	Spleen	Thoracic Aorta
Target Image 0	0.973	0.907	0.923	0.896
Target Image 1	0.968	0.874	0.921	0.888
Target Image 2	0.973	0.864	0.935	0.908
Target Image 3	0.962	0.839	0.946	0.886
Target Image 4	0.968	0.868	0.923	0.907

is well segmented. This may be due to the intrinsic property, which favors large objects instead of small objects.

Some future improvement can be done by incorporating shape constraints or using a better model (atlas). Shape constraint can prevent the contour being attracted to some undesired edge. A better model which is similar to the input images requires less initialization work and can attain better segmentation accuracy.

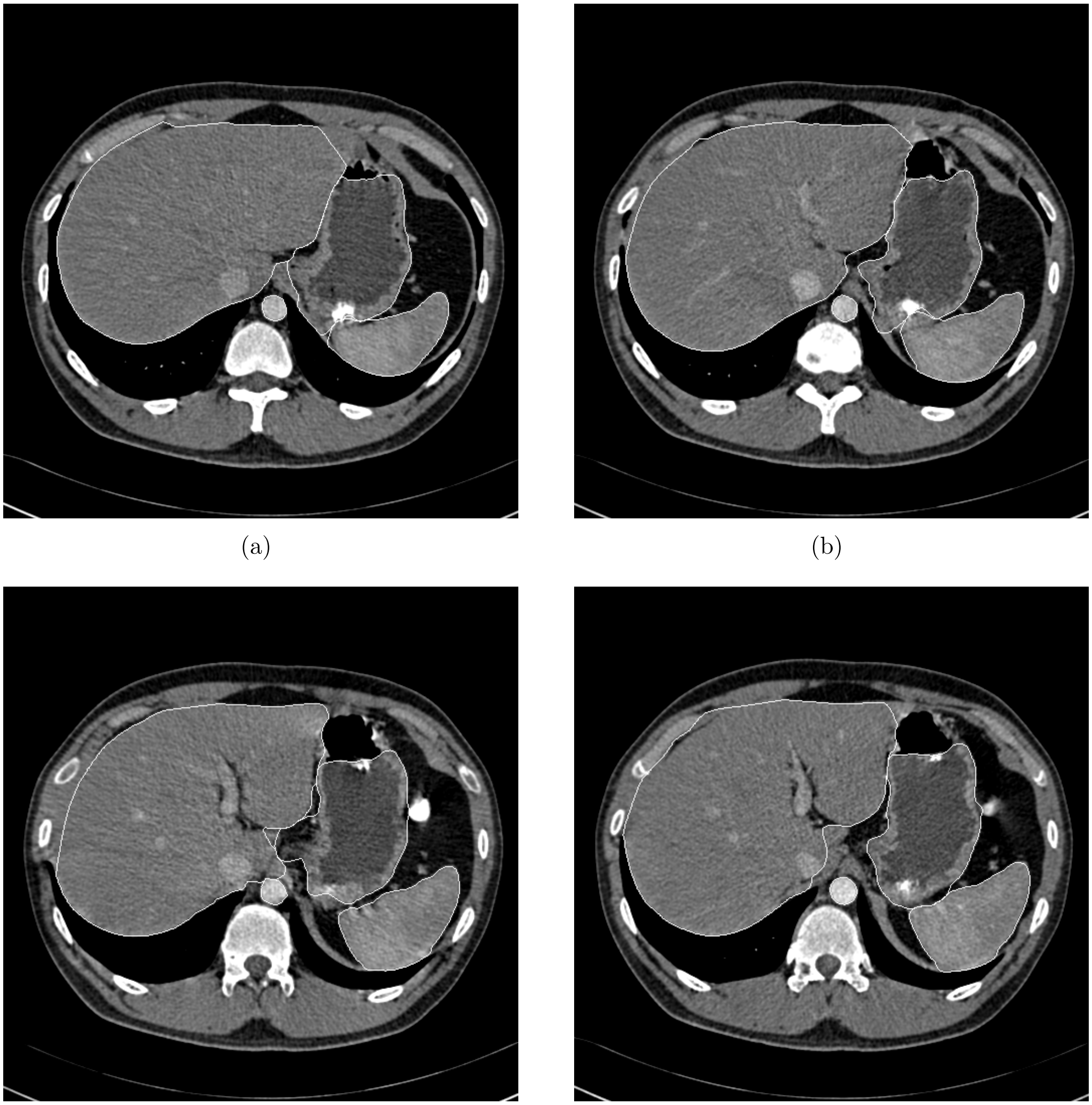

(a) (b)

(c) (d)

Figure 4.5: More results of different input CT images. (a), (b), (c) and (d) are results for input image 0, 1, 3 and 4, respectively. Livers, stomachs, spleens and thoracic aortae are enclosed in white contours.

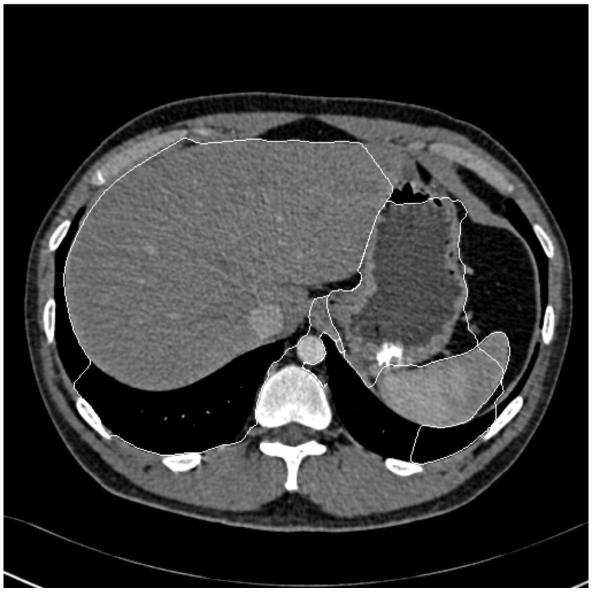

Figure 4.6: Final result without local transformation. The red contour is supposed to enclose the liver part. The yellow contour is supposed to enclose the stomach part. The blue contour is supposed to enclose the spleen part. The green contour is supposed to enclose the thoracic aorta part. But they are more or less attracted to the wrong edges.

Chapter 5

Conclusions

In this paper, a thorough review of generic image segmentation approaches and the approaches employed for medical image segmentation is presented.

The generic segmentation algorithms are categorized into five classes, namely thresholding approaches[36, 7, 33, 37], region-based approaches [2, 10, 39, 47, 5, 31, 18, 27], edge-based approaches [17, 8], graph-based approaches [45, 38, 43] and classification-based approaches [6, 30, 14]. Their algorithms are analyzed. A comparison shows that generic segmentation algorithms are based on either pixel information or local patch information. Their computational complexities are relatively low. They are usually easy to use. However, they are all sensitive to noise. They tend to over segment the images. Moreover, the segmentation results may not correspond to the desired object.

The medical segmentation approaches are categorized into two classes, namely deformable model approaches and atlas-based approaches. The deformable model approaches contain numerous models such as active contour model (snake) [22, 3, 15], gradient vector flow [46], level set [35, 24], active shape model [20, 12, 44, 16] and other free-form models [40, 21, 25, 19, 26]. The deformable models are the most popular approaches currently used in medical image segmentation. Atlas-based approaches [11, 13, 29, 41, 1] are prosperous for its ability to incorporate prior information. These medical image segmentation approaches have the advantage of generating continuous contours. However, they are usually computationally expensive. They are also sensitive to noise. Snake-based algorithms are easily fooled by the edges produced by noise. In addition, most of them are sensitive to the initial configurations of the contours.

The review shows that each of the existing methods, by itself, cannot solve the segmentation problem defined in Chapter 1. They must be combined together to form a reasonable solution. Even within each approach itself, it also incorporates some other approaches. For instance, the atlas-based approaches incorporate deformable models to deform the atlas, the deformable model approaches use the edge/region information in the images etc.

The review shows atlas-based segmentation algorithm is prosperous. Besides the advantages of other medical segmentation approaches, it can also provide rough initial configurations of the contours. It can also incorporate probability distribution of the contours based on a series of training data. However, atlas-based approach has the assumption that the model image and input images should be similar. Some possible research topics on atlas-based segmentation are proposed, either to improve the approach itself, or to find some ways to build a "good" model.

A preliminary work is presented in this paper, which is mainly based on atlas-based segmentation. The proposed algorithm tries to initialize the atlas contours by global transformation and local transformation, and feeds the transformed contours into the standard GVF snake program to refine the contour. The results show that atlas-based segmentation approach has at least the potential to solve the segmentation problem given that the model image and input image are similar.

Bibliography

[1] Georges B. Aboutanos, Jyrki Nikanne, Nancy Watkins, and Benoit M. Dawant. Model creation and deformation for the automatic segmentation of the brain in MR images. *IEEE Transactions on Biomedical Engineering*, 46(11):1346–1356, November 1999.

[2] Rolf Adams and Leanne Bischof. Seeded region growing. *IEEE Transaction on Pattern Analysis and Machine Intelligence*, 16(6):641–647, June 1994.

[3] M. Stella Atkins and Blair T. Mackiewich. Fully automated hybird segmentation of the brain. In Issac N. Bankman, editor, *Handbook of Medical Imaging, Processing and Analysis*, chapter 11, pages 171–183. Academic Press, 2000.

[4] Isaac N. Bankman, editor. *Handbook of Medical Imaging.* Academic Press, 2000.

[5] S. Beucher and C. Lantuéjoul. Use of watersheds in contour detection. In *Proc. International Workshop on Image Processing, Real-Time Edge and Motion Detection/Estimation*, September 1979.

[6] Matthew S. Brown, Michael F. Mcnitt-Gray, Jonathan G. Goldin Nicholas J. Mankovich, John Hiller, Laurence S. Wilson, and Denise R. Aberle. Method for segmenting chest CT image data using an anatomical model: Preliminary results. *IEEE Transactions on Medical Imaging*, 16(6):828–839, 1997.

[7] Jinhai Cai and Zhi-Qiang Liu. A new thresholding algorithm based on all-pole model. In *Pattern Recognition, International Conference on*, pages 34–36, August 1998.

[8] J. Canny. A computational approach to edge detection. *IEEE Transactions on Pattern Analysis and Machine Intelligence*, 8(6):679–698, November 1986.

[9] Vikram Chalana and Yongmin Kim. A methodology for evaluation of boundary detection algorithms on medical images. *Medical Imaging, IEEE Transactions on*, 16(5):642–652, Oct. 1997.

[10] P. Chen and T. Pavlidis. Image segmentation as an estimation problem. *Computer Graphics and Image Processing*, 12:153–172, 1980.

[11] D. Louis Collins, Alex P. Zijdenbos, Wim F. C. Baaré, and Alan C. Evans. ANIMAL+INSECT : Improved cortical structure segmentation. In Attila Kuba, Martin Sámal, and Andrew Todd-Pokropek, editors, *PIMI*, volume 1613, pages 210–223. Springer, 1999.

[12] T. F. Cootes, A. Hill, C. J. Taylor, and J.Haslam. The use of active shape models for locating structures in medical images. *Image and Vision computing*, 12(6):355–366, July 1994.

[13] Valérie Duay, Nawal Houhou, and Jean-Philippe Thiran. Atlas-based segmentation of medical images locally constrained by level sets. Technical Report 07/2005, Signal Processing Institute, Ecole Polytechnique Fédérale de Lausanne, CH-1015 Lausanne, Switzerland, February 2005.

[14] Jie Feng, Wei-Chung Lin, and Chin-Tu Chen. Epicardial boundary detection using fuzzy reasoning. *Medical Imaging, IEEE Transactions on*, 10(2):187–199, June 1991.

[15] Jean Gao, Akio Kosaka, and Avi Kak. A deformable model for human organ extraction. In *ICIP 98*, volume 3, pages 323–327, October 1998.

[16] S. S. Gleason, H. Sari-Sarraf, M. A. Abidi, O. Karakashian, and F. Morandi. A new deformable model for analysis of X-Ray CT images in preclinical studies of mice for polycystic kidney disease. *IEEE Transactions on Medical Imaging*, 21(10):1302–1309, October 2002.

[17] Rafael C. Gonzalez and Richard E. Woods. *Digital Image Processing*. Prentice Hall, 2001.

[18] V. Grau, A.U.J. Mewes, M. Alcañiz, R. Kikinis, and S.K. Warfield. Improved watershed transform for medical image segmentation using prior information. *IEEE Transaction on Medical Imaging*, 23(4):447–458, 2004.

[19] Robert P. Grzeszczuk and David N. Levin. "Brownian Strings": Segmenting images with stochastically deformable contours. *IEEE Transactions on Pattern Analysis and Machine Intelligence*, 19(10):1100–1114, October 1997.

[20] A. Hill, C. J. Taylor, and T. Cootes. Object recognition by flexible template matching using genetic algorithms. In *European Conference on Computer Vision*, pages 852–856, May 1992.

[21] Lawrence H.Staib and James S. Duncan. Model-based deformable surface finding for medical images. *IEEE Transcations on Medical Imaging*, 15(5):720–731, October 1996.

[22] Michael Kass, Andrew Witkin, and Demetri Terzopoulos. Snakes: Active contour models. *Int'l J. Computer Vision*, pages 321–331, 1987.

[23] M. Kaus, S. K. Warfield, F. A. Jolesz, and R. Kikinis. Adaptive template moderated brain tumor segmentation in MRI. In *Bildverarbeitung fur die Medizin*, pages 102–106. Springer Verlag, 1998.

[24] Ravikanth Malladi, James A. Sethian, and Baba C. Vemuri. Shape modeling with front propagation: A level set approach. *IEEE Transactions on Pattern Analysis and Machine Intelligence*, 17(2):158–175, February 1995.

[25] David Mattes, David R. Haynor, Hubert Vesselle, Thomas K. Lewellen, and William Eubank. PET-CT image registration in the chest using free-form deformations. *IEEE Transactions on Medical Imaging*, 22(1):120–128, January 2003.

[26] Dimitris N. Metaxas and Ioannis A. Kakadiaris. Elastically adaptive deformable models. *IEEE Transactions on Pattern Analysis and Machine Intelligence*, 24(10):1310–1321, October 2002.

[27] L. Najman and M. Schmitt. Geodesic saliency of watershed contours and hierarchical segmentation. *Pattern Analysis and Machine Intelligence, IEEE Transactions on*, 18, Dec 1996.

[28] L. O'Gorman and A. C. Sanderson. The converging squares algorithm: An efficient multidimensional peak picking method. In *International Conference on Acoustics, Speech, and Signal Processing*, volume 8, pages 112–115, April 1983.

[29] Hyunjin Park, Peyton H. Bland, and Charles R. Meyer. Construction of an abdominal probabilistic atlas and its application in segmentation. *IEEE Transactions on Medical Imaging*, 22(4):483–492, April 2003.

[30] Xiaofeng Ren and Jitendra Malik. Learning a classification model for segmentation. In *International Conference on Computer Visioin*, Nice, France, October 2003.

[31] Jos B.T.M. Roerdink and Arnold Meijster. The watershed transform: Definitions, algorithms and parallelization strategies. *Fundamenta Informaticae*, 41, 2001.

[32] Jadwiga Rogowska. Overview and fundamentals of medical image segmentation. In Isaac N. Bankman, editor, *Handbook of Medical Imaging, Processing and Analysis*, chapter 5, pages 69–85. Academic Press, 2000.

[33] Prasanna Sahho, Carrye Wilkins, and Jerry Yeager. Threshold selection using renyi's entropy. *Pattern Recognition*, 30(1):71–84, 1997.

[34] J. Serra. *Image Analysis and Mathematical Morphology.* Academic Press, 1982.

[35] J. A. Sethian. *Level Set Methods.* Cambridge University Press, 1996.

[36] Mehmet Sezgin and Bülent Sankur. Survey over image thresholding techniques and quantitative performance evaluation. *Journal of Electronic Imaging*, 13(1):146–165, January 2004.

[37] V. A. Shapiro, P. K. Veleva, and V. S. Sgurev. An adaptive method for image thresholding. In *Pattern Recognition, International Conference on*, volume III, pages 696–699, April 1992.

[38] Jianbo Shi and Jitendra Malik. Normalized cuts and image segmentation. *IEEE Transactions on Pattern Analysis and Machine Intelligence*, 22(8):888–905, August 2000.

[39] M. Spann and R. Wilson. A quad-tree approach to image segmentation which combines statistical and spatial information. *Pattern Recogition*, 18:257–269, 1984.

[40] Lawrence H. Staib and James S. Duncan. Boundary finding with parametrically deformable models. *IEEE Transactions on Pattern Analysis and Machine Intelligence*, 14(11):1061–1075, November 1992.

[41] Matús Straka, Alexandra La Cruz, Arnold Köchl, Milos Srámek, Meister Eduard Gröller, and Dominik Fleischmann. 3d watershed transform combined with a probabilistic atlas for medical image segmentation. In *MIT 2003*, pages

[42] D. L. Toulson and J. F. Boyce. Segmentation of MR image using neural nets. In *Image and Vision Computing*, volume 10, pages 324–328, 1992.

[43] Song Wang and Jeffrey Mark Siskind. Image segmentation with ratio cut. *IEEE Transcations on Pattern Analysis and Machine Intelligence*, 25(6):675–690, June 2003.

[44] Yongmei Wang and Lawrence H. Staib. Boundary finding with correspondence using statistical shape models. In *Computer Vision and Pattern Recognition*, pages 338–345, June 1998.

[45] Zhenyu Wu and Richard Leahy. An optimal graph theoretic approach to data clustering: Thoery and its application to image segmentation. *IEEE Transactions on Pattern Analysis and Machine Intelligence*, 15(11):1101–1113, November 1993.

[46] Chenyang Xu and Jerry L. Prince. Snakes, shapes, and gradient vector flow. *IEEE Transaction on Image Processing*, 7(3), March 1998.

[47] Xiaohan Yu, Juha Ylä-Jääski, Olli Huttunen, Tuomo Vehkomäki, Outi Sipilä, and Toivo Katila. Image segmentation combining region growing and edge detection. In *Pattern Recognition, International Conference on*, volume III, pages 481–484, April 1992.

[48] Alex P. Zijdenbos, Benoit M. Dawant, Richard A. Margolin, and Andrew C. Palmer. Morphometric analysis of white matter lesions in MR images: Method and validation. *IEEE Transcations on Medical Imaging*, 13(4):716–724, December 1994.